Article

Comparison of NH$_3$ and N$_2$O Plasma Treatments on Bi$_2$O$_3$ Sensing Membranes Applied in an Electrolyte–Insulator–Semiconductor Structure

Chyuan-Haur Kao [1,2,3], Kuan-Lin Chen [1], Yi-Shiang Chiu [4], Lin Sang Hao [4], Shih-Ming Chen [4], Ming-Hsien Li [4], Ming-Ling Lee [5,*] and Hsiang Chen [4,*]

[1] Department of Electronic Engineering, Chang Gung University, 259 Wen-Hwa 1st Road, Kwei-Shan District, Taoyuan City 333, Taiwan; chkao@mail.cgu.edu.tw (C.-H.K.); chkao@mail.cgu.edu (K.-L.C.)
[2] Kidney Research Center, Department of Nephrology, Chang Gung Memorial Hospital, Chang Gung University, No. 5 Fuxing Street, Guishan District, Taoyuan City 333, Taiwan
[3] Department of Electronic Engineering, Ming Chi University of Technology, 284 Gungjuan Road, Taishan District, New Taipei City 243, Taiwan
[4] Department of Applied Materials and Optoelectronic Engineering, National Chi Nan University, Puli, Nantou 545, Taiwan; s109328018@mail1.ncnu.edu.tw (Y.-S.C.); s109328023@mail1.ncnu.edu.tw (L.S.H.); s107328009@mail1.ncnu.edu.tw (S.-M.C.); mhli1125@ncnu.edu.tw (M.-H.L.)
[5] Department of Electro-Optical Engineering, Minghsin University of Science and Technology, No. 1, Xinxing Road, Xinfeng, Hsinchu 30401, Taiwan
[*] Correspondence: mingling@must.edu.tw (M.-L.L.); hchen@ncnu.edu.tw (H.C.)

Abstract: In this study, bismuth trioxide (Bi$_2$O$_3$) membranes in an electrolyte–insulator–semiconductor (EIS) structure were fabricated with pH sensing capability. To optimize the sensing performance, the membranes were treated with two types of plasma—NH$_3$ and N$_2$O. To investigate the material property improvements, multiple material characterizations were conducted. Material analysis results indicate that plasma treatments with appropriate time could enhance the crystallization, remove the silicate and facilitate crystallizations. Owing to the material optimizations, the pH sensing capability could be greatly boosted. NH$_3$ or N$_2$O plasma treated-Bi$_2$O$_3$ membranes could reach the pH sensitivity around 60 mV/pH and show promise for future biomedical applications.

Keywords: bismuth trioxide; plasma treatment; NH$_3$ and N$_2$O; nitrogen passivation; grainization

1. Introduction

Fifty years ago, the first ion-sensitive field-effect transistor (ISFET) was invented by Bergveld in 1970 [1,2]. Following the invention, semiconductor-based ion sensing technology [1–3] has been developed since the late 20th century. Among various types of ion sensing semiconductor devices, electrolyte–insulator–semiconductor (EIS) sensors with rapid response, high reliability and simple structure have been intensively studied [4]. Because of low capacitance and poor electrochemical properties, SiO$_2$ has been replaced by various oxides to improve the membranes properties [5]. Recently, Ta$_2$O$_5$ [6], WO$_3$ [7], and La$_2$O$_3$ [8] have emerged as novel membrane materials [9]. However, to further boost the membrane sensing performance, novel materials and new treatments are worthwhile to be explored. Bismuth trioxide (Bi$_2$O$_3$) with a bandgap around 2.5 eV has been utilized as photocatalyst [10], super capacitors, and gas sensor materials [11]. However, Bi$_2$O$_3$-based pH sensing membranes [12] have not been clearly reported, yet. Furthermore, to enhance the sensing capability, Bi$_2$O$_3$ membranes were treated with two types of plasma-NH$_3$ and N$_2$O [13,14]. To investigate the improvement of the treatment, multiple material analysis techniques including X-ray diffraction (XRD), X-ray photoelectron spectroscopy (XPS), atomic force microscopy (AFM), and secondary ion mass spectrometry (SIMS) were performed. Material analysis results indicate that Bi$_2$O$_3$ membranes treated with NH$_3$

plasma for 3 min and N_2O plasma for 1 min had strong crystallization, silicate suppression, high grainization, and effective nitrogen passivation. Moreover, the pH sensing measurements [15] indicate that Bi_2O_3 membranes treated in these plasma treatment conditions had high pH sensitivity around 60 mV/pH and high linearity close to 100%. Hysteresis and drift [16] rate evaluation also reveal that the membrane treated in these conditions had the lowest hysteresis voltage and the smallest drift rate. NH_3 and N_2O plasma treatments could incorporate the nitrogen atoms into the deep part of the devices to fix the defects and eliminate the silicates.

According to previous reports [17,18], plasma treatment can eliminate the silicate layer because, because silicates can have chemical reaction and transform from SiOx with dangling bonds to Si–O–Si bonds. The atoms in the plasma such as F or N can facilitate the combination of the silicon or oxygen dangling bonds to form well-crystallized Si–O–Si [19]. Therefore, silicate can be reduced, and near-perfect crystals can replace the silicate. The effective electric field across the membranes can be enhanced so the sensing capability can be improved [20,21]. Moreover, the nitrogen incorporation in the bulks may form NH_2 bond to strengthen the chemical bonds and improve the material properties [22]. On the other hand, plasma treatment of the sensing film could cause an EIS structure sensitive to H^+ ions [23] because the increase of the metal ions produced on the surface sites to decrease the diffusion capacitance in the solution and enhance the sensitivity. Furthermore, based on the Gouy–Chapman–Stern model [24,25], the sensing parameter β is proportional to the density of surface states, as shown in (1), where Ns is the number of surface sites per unit surface area and C_{DL} is the double layer capacitance. Therefore, the sensing capability can be enhanced by NH_3 and N_2O plasma treatments.

$$\beta = \frac{2q^2 Ns \sqrt{K_a K_b}}{KT C_{DL}} \tag{1}$$

Owing to high sensitivity, fair linearity, stable response, Bi_2O_3-based EIS membranes [26] with NH_3 or N_2O plasma treatments show promise for future industrial biomedical sensing [27] applications.

2. Experimental

To prepare the EIS sensor with Bi_2O_3 sensing film, 3.95 g of bismuth nitrate ($Bi(NO_3)_3 \cdot 5H_2O$) was dissolved in 20 mL of nitric acid with the solution concentration of 1 M. The sol-gel solution was dropped onto the cleansed p-Si substrate. Then, a Bi_2O_3 film formed on it, and then the plasma treatments were performed. The samples were treated with NH_3 and N_2O plasma at 100 W RF power and 500 mTorr processing pressure for 1 min, 3 min, and 6 min, respectively. Then, an Al film with a thickness of 300 nm was deposited on the back of the silicon wafer and the silicone glue was used to define the sensing window, and the device was glued to be fixed on a PCB board. Finally, AB glue was used for packaging to prevent oxidation. The device structure is illustrated in Figure 1.
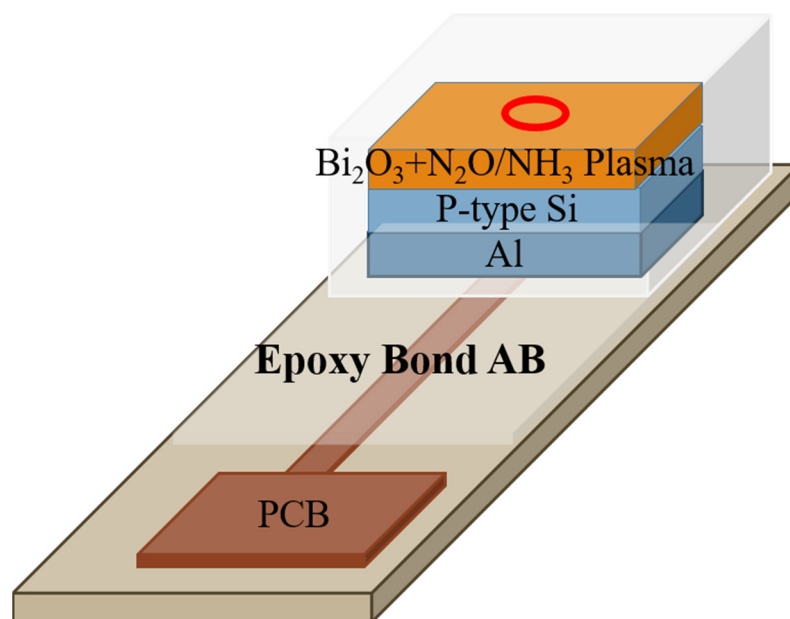
**Figure 1.** A Bi_2O_3-based membrane in an EIS structure with plasma treatments.

3. Results and Discussion

To examine the crystalline structures of the membranes, XRD was used. Figure 2a shows the X-ray diffraction patterns of Bi_2O_3 film after NH_3 plasma treatments for various times. The two diffraction peaks BiO (012) and Bi_2O_3 (200) are located at 27.8° and 32.6°, respectively. The as-deposited sample shows a peak of BiO. After NH_3 plasma treatment for 3 min, the sample shows the strongest peak of Bi_2O_3 (200) among all the samples.
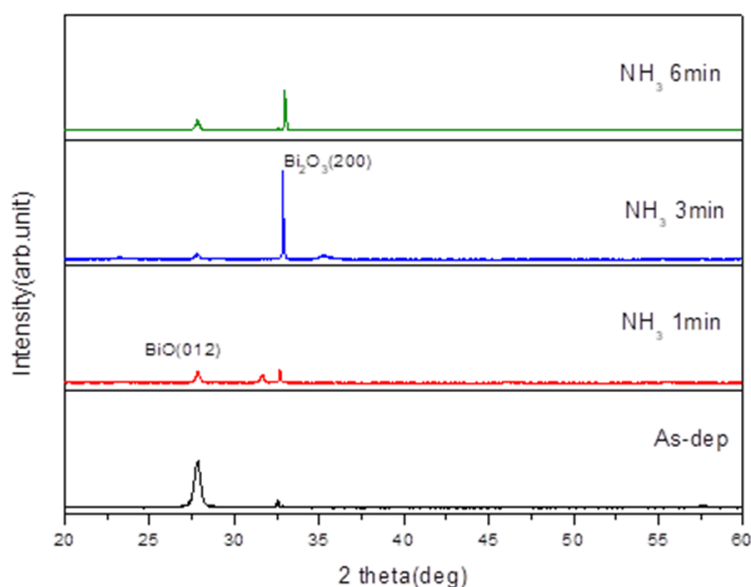
(a)

Figure 2. *Cont*.
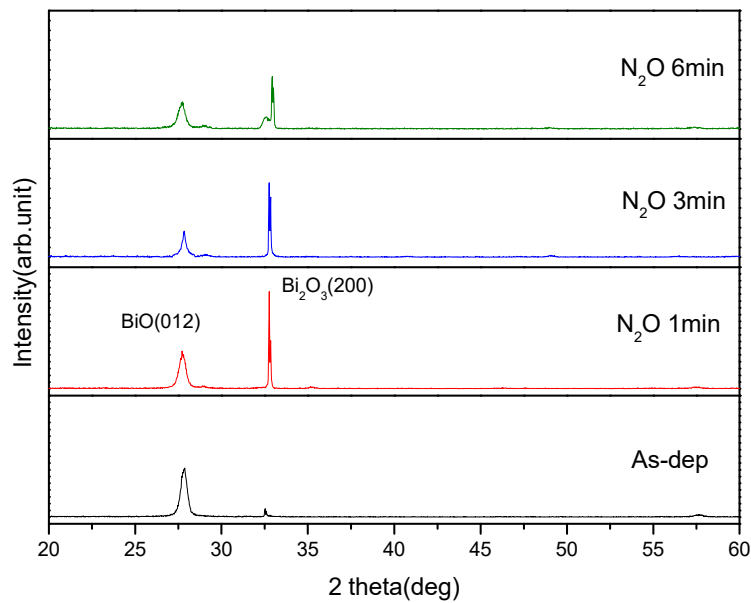
(b)

Figure 2. XRD patterns of the Bi_2O_3 film after (**a**) NH_3 and (**b**) N_2O plasma treatments for various time.

By contrast, Figure 2b shows the X-ray diffraction analysis of the Bi_2O_3 film after N_2O plasma treatments for various times. The diffraction peaks BiO (012) and Bi_2O_3 (200) are located at 27.8° and 32.6°, respectively. The as-deposited sample also shows a peak of BiO. After N_2O plasma treatment for 1 min, the sample shows the strongest Bi_2O_3 (200) peak among all the samples. With the increase of the plasma treatment time, the intensity of the Bi_2O_3 (200) peak gradually decreased.

Furthermore, XPS analysis was used to study the chemical bonding state of the Bi_2O_3 sensor film after NH_3 and N_2O plasma treatments. The O1s spectra of the samples after NH_3 plasma treatments is shown in Figure 3a. The as-deposited and annealed samples have 4 peak fitting curves, namely SiO_2 (531.8 eV), silicate (531.4 eV), oxygen defect (530.3 eV), and Bi-O (529 eV). After the NH_3 plasma treatment, the oxygen defects and slicates were significantly reduced. Because NH_3 plasma treatment could dope N into the film to improve dangling bonds and strain bonds, the sensing properties were improved.

The O1s spectra of the samples after N_2O plasma treatment is shown in Figure 3b. The as-deposited and annealed samples have three peak fitting curves, namely, silicate (531.4 eV), oxygen defect (530.3 eV), and Bi-O (529 eV). After N_2O plasma treatment, the oxygen defects and silicates were significantly suppressed. Since N_2O plasma treatment could incorporate N into the film, mitigate dangling bonds and strain bonds, and strengthen the film structure, the sensing behaviors could be improved. Results indicate that N atoms in the plasma could transform SiO_x with dangling bonds to form well-crystallized Si–O–Si.

Figure 4a–d shows the atomic force microscope (AFM) images of the Bi_2O_3 film after NH_3 plasma treatments for various times, and Figure 4e–h shows the atomic force microscope (AFM) images of the Bi_2O_3 film after N_2O plasma treatments for various times. The root mean square (Rms) roughness of the sample without plasma treatment and of the samples after NH_3 plasma treatment for 1, 3, and 6 min were 1.31, 5.32, 15.56, and 11.33 nm, respectively. The root mean square (Rms) roughness of the sample without plasma treatment and of the samples after N_2O plasma treatment for 1, 3, and 6 min were 1.31, 3.9, 3.83, and 3.21 nm, respectively. After 3 min of NH_3 plasma treatment of 1 min of N_2O plasma treatment, the Bi_2O_3 film has the largest Rms value. The incorporation of N can passivate the defects improve the crystalline structure, and strengthen the grainization, thereby increasing the surface sites and improving the sensing characteristics.
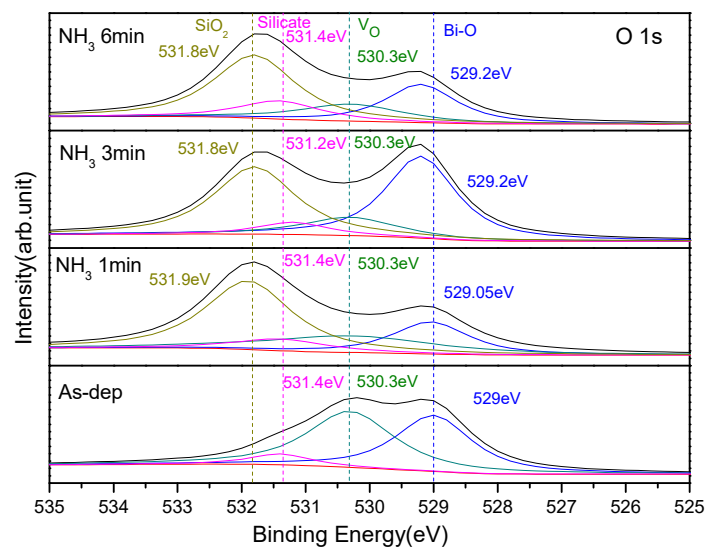
(**a**)
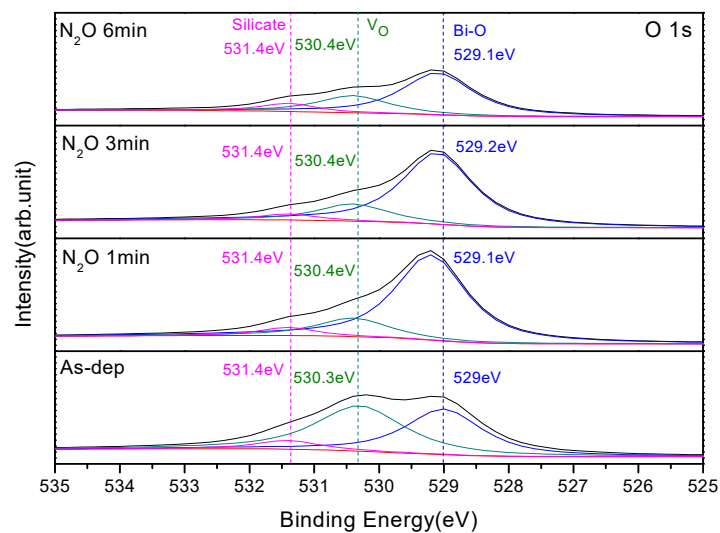
(**b**)

Figure 3. The O1s XPS spectra of the Bi_2O_3 film after (**a**) NH_3 and (**b**) N_2O plasma for various treatment time.

To examine the surface morphologies, Figure 5a–f shows the field emission scanning electron microscope (FESEM) images of the deposited Bi_2O_3 film and the Bi_2O_3 film after NH_3 and N_2O plasma treatments. After 1 min of NH_3 plasma treatment, irregular crystals with uneven distribution were produced on the surface. After 3 min of plasma treatment, the crystals became denser. After 6 min of plasma treatment, the crystals became sparsely distributed again. Therefore, the NH_3 plasma treatment in 3 min had the best material properties. (FESEM) images of the deposited Bi_2O_3 film and the Bi_2O_3 film before and after N_2O plasma treatment for 1 min are shown in Figure 5e,f. After N_2O plasma treatments for 1 min, the crystallization of the film became obvious. Due to the incorporation of N, the dangling bonds and strain bonds in the film can be fixed, and the crystalline structure could be strengthened, so the sensing could be improved.
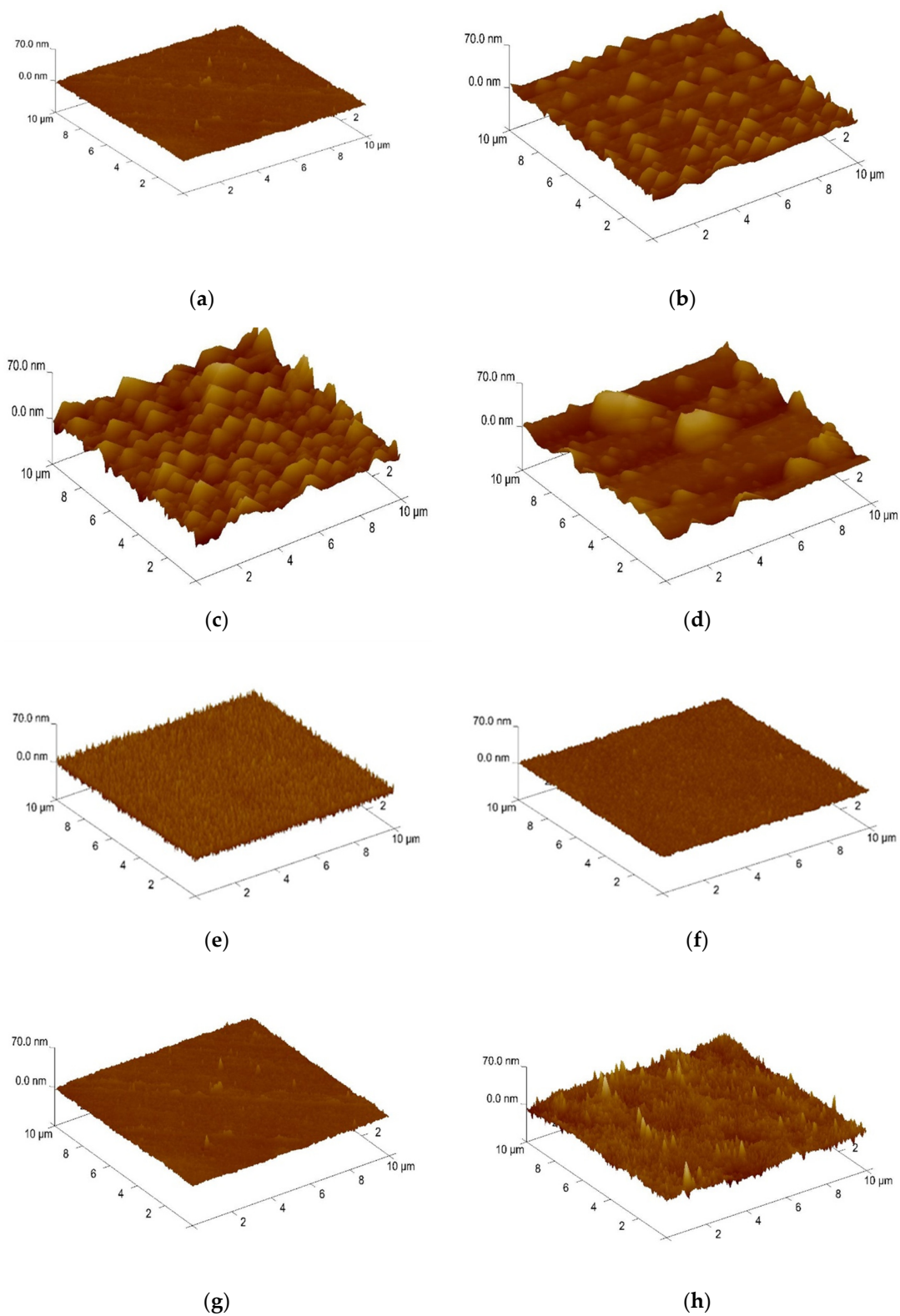
(**a**)

(**b**)

(**c**)

(**d**)

(**e**)

(**f**)

(**g**)

(**h**)

Figure 4. Three-dimensional (3D)-AFM images of Bi_2O_3 film after NH_3 plasma treatment for (**a**) 0 min RMS:1.31 nm; (**b**) 1 min NH_3 plasma RMS: 5.32 nm; (**c**) 3 min NH_3 plasma RMS: 15.56 nm; (**d**) 6 min NH_3 plasma RMS: 11.33 nm. Three-dimensional (3D)-AFM of Bi_2O_3 film after different N_2O plasma treatment for (**e**) 0 min RMS:1.31 nm; (**f**) 1 min N_2O plasma RMS: 3.9 nm; (**g**) 3 min N_2O plasma RMS: 3.83 nm; (**h**) 6 min N_2O plasma RMS: 3.21 nm.

(**a**)

(**b**)

(**c**)

(**d**)

(**e**)

(**f**)
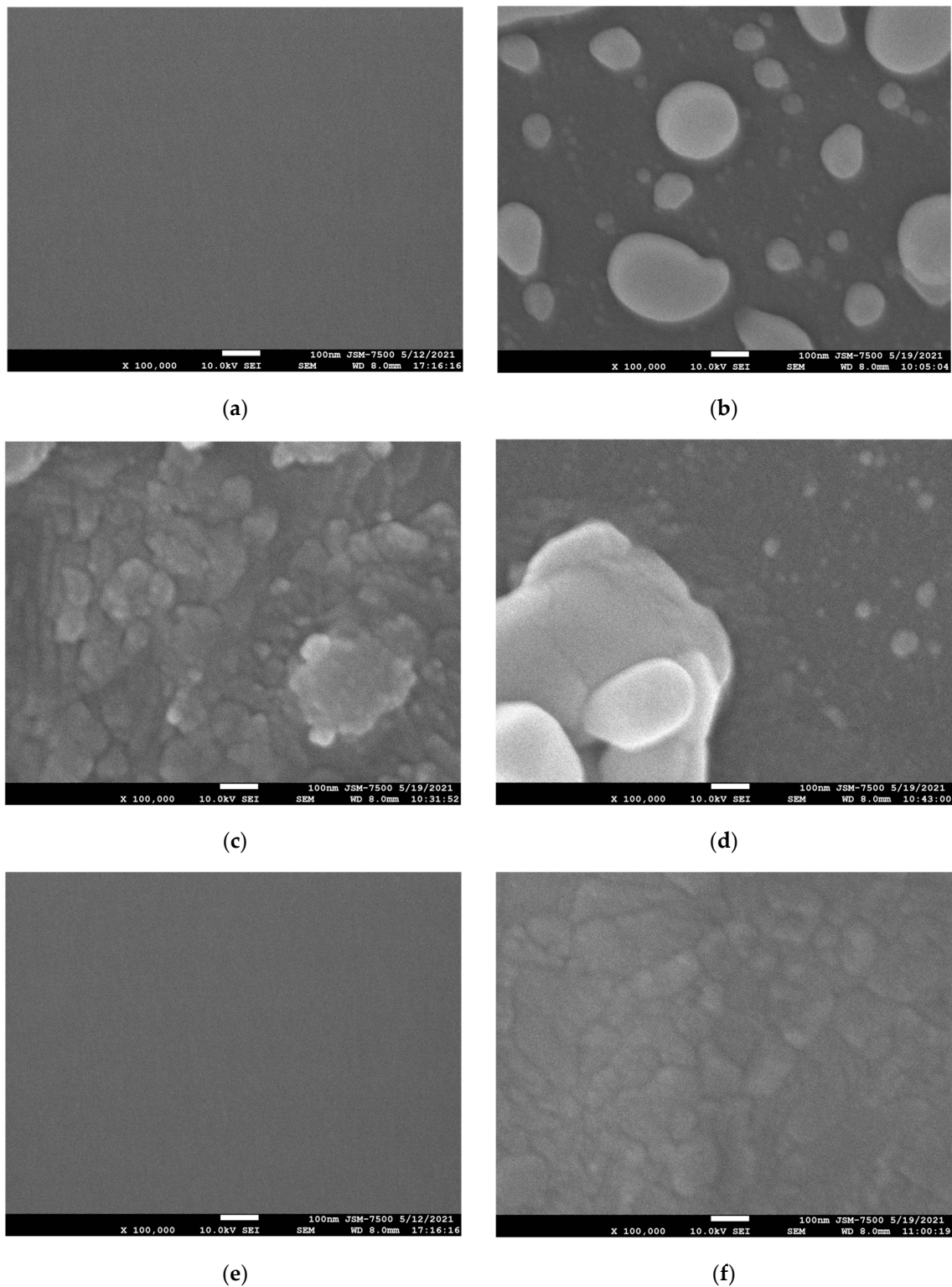
Figure 5. FESEM of Bi_2O_3 film after different NH_3 and N_2O plasma treatment times: (**a**) As-dep; (**b**) 1 min NH_3 plasma; (**c**) 3 min NH_3 plasma; (**d**) 6 min NH_3 plasma; (**e**) As-dep; (**f**) 1 min N_2O plasma.

In addition, the images of the two types of plasma treatments are compared. It can be found that the uniformity of the film after N_2O plasma treatments is more uniform than that of the Bi_2O_3 film after NH_3 plasma treatment. Therefore, Bi_2O_3 film maybe more stable after N_2O plasma treatments than NH_3 plasma treatments.

Figure 6a,b shows the SIMS of the samples with NH_3 and N_2O plasma treatment for various time. It can be seen that as the plasma treatment time increased, the thickness of the sensing film decreased. As the film after plasma treatment would be etched with the increase of the plasma treatment time, the sensing characteristics were slightly reduced. On the other hand, nitrogen atoms can be introduced into the Bi_2O_3/Si interface by NH_3 and N_2O plasma treatment as shown in the two SIMS profiles. These accumulated nitrogen atoms can passivate the defects of the interface. Since the incorporation of N can improve the dangling bonds and strain bonds of the film, the sensing performance is improved.
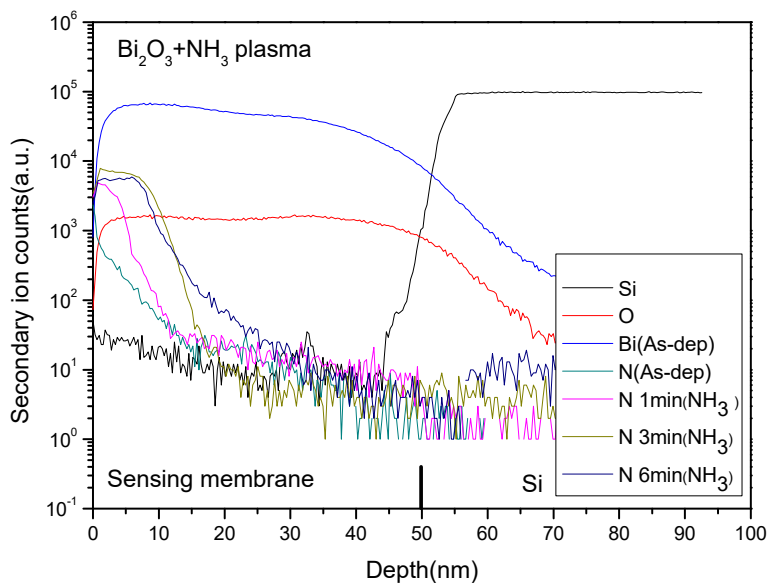

(**a**)
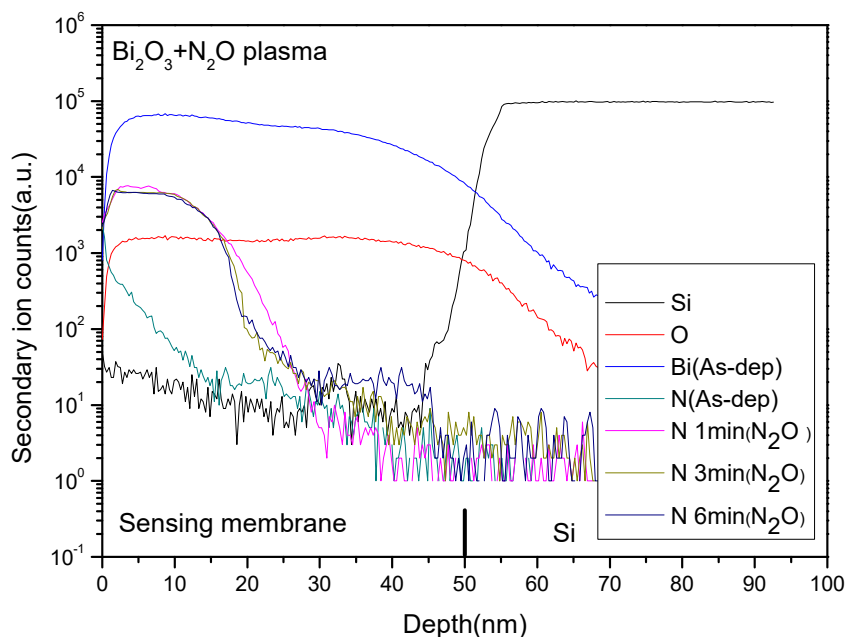
(**b**)

Figure 6. SIMS analysis for Bi_2O_3 film after: (**a**) NH_3 plasma treatments; (**b**) N_2O plasma treatments for various time.

As the two plasma treatments are compared, it can be found that the amount of nitrogen incorporated after the N_2O plasma treatment was relatively stable, and the nitrogen content only slightly decreased with the increase of the plasma time. Therefore, the N_2O plasma treatment had relatively stable sensing characteristics.

To assess the pH sensing behaviors, C–V curves of Bi_2O_3 after different NH_3 and N_2O plasma treatment conditions were measured. Figure 7a–d shows C–V curves of Bi_2O_3 after NH_3 plasma for various times. The sensitivity value without NH_3 plasma treatment was 42.66 mV/pH, and the linearity was 94.483%. After NH_3 plasma treatment for 1 min, 3 min and 6 min, the sensitivity values became 30.87, 59.84 and 40.83 mV/pH, respectively, and the linearity values became 84.45%, 99.25% and 97.17%. As for the sensitivity among the Bi_2O_3 samples with different NH_3 plasma time, it can be found that the Bi_2O_3 sensor film had the highest sensitivity after NH_3 plasma treatment for the 3 min sample. Consistent with the FESEM images, the film treated in this condition produced densely arranged and layered crystals, which produced a larger contact area and increased sensitivity. After 3 min of NH_3 plasma treatment, there were small and dense Bi_2O crystals, thereby increasing the sensitivity of the sensing film.

Figure 7e–h shows the C–V curve of Bi_2O_3 after different N_2O plasma treatment time. After N_2O plasma treatment for 1 min, 3 min and 6 min, the sensitivity were 60.43, 59.91 and 59.8 mV/pH, respectively. The linearity was 99.82%, 98.97% and 99.64%. As for the sensitivity of Bi_2O_3 under different N_2O plasma time, it can be found that the sensitivity of the Bi_2O_3 film after N_2O plasma for various times and the samples in all the conditions were improved, consistent with FESEM images of the uniform distributed crystals under various plasma treatment conditions. After N_2O plasma treatment, surface defects could be passivated, and dangling bonds and strain bonds can be fixed. Therefore, plasma treatments could improve the material properties and enhance the crystalline structure and grainization effect, and thereby increasing sensitivity.
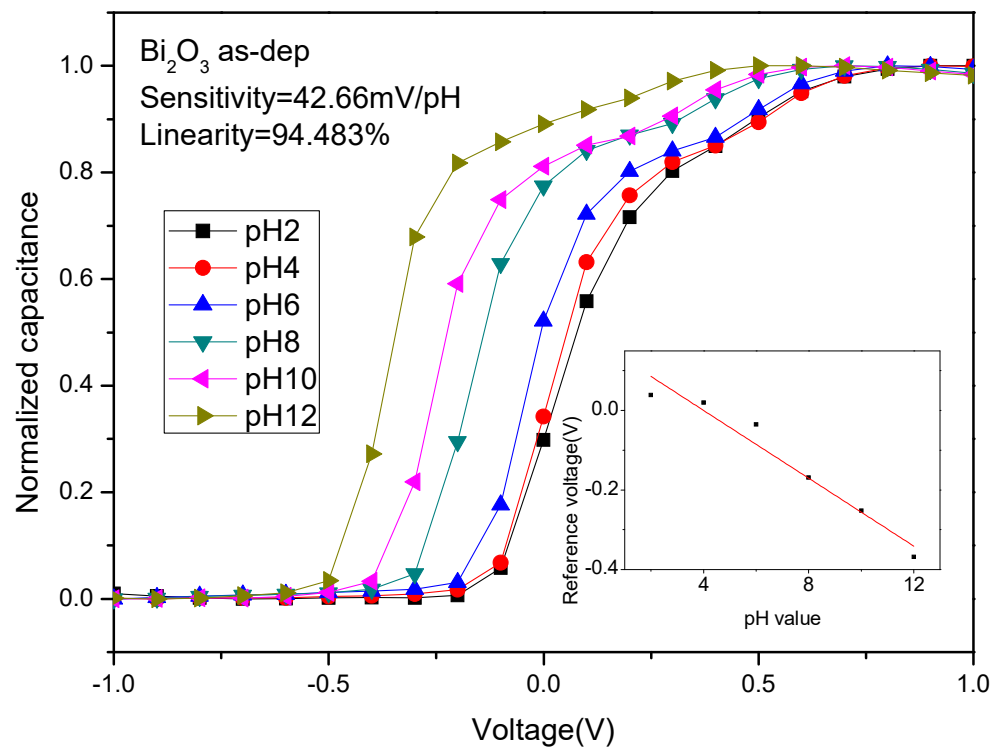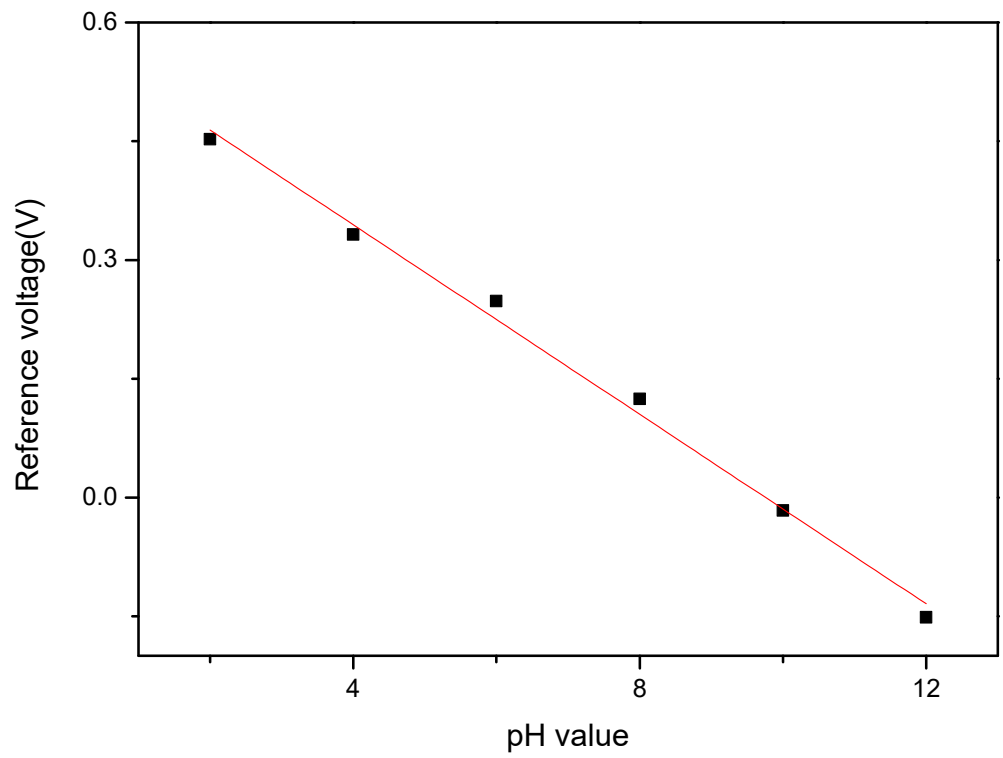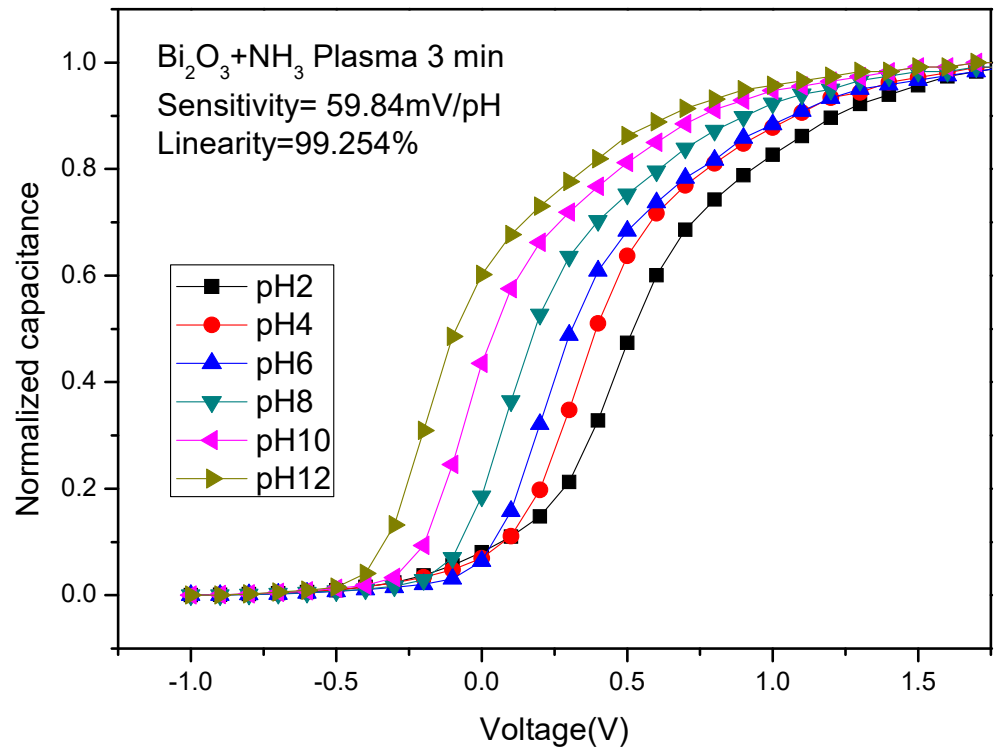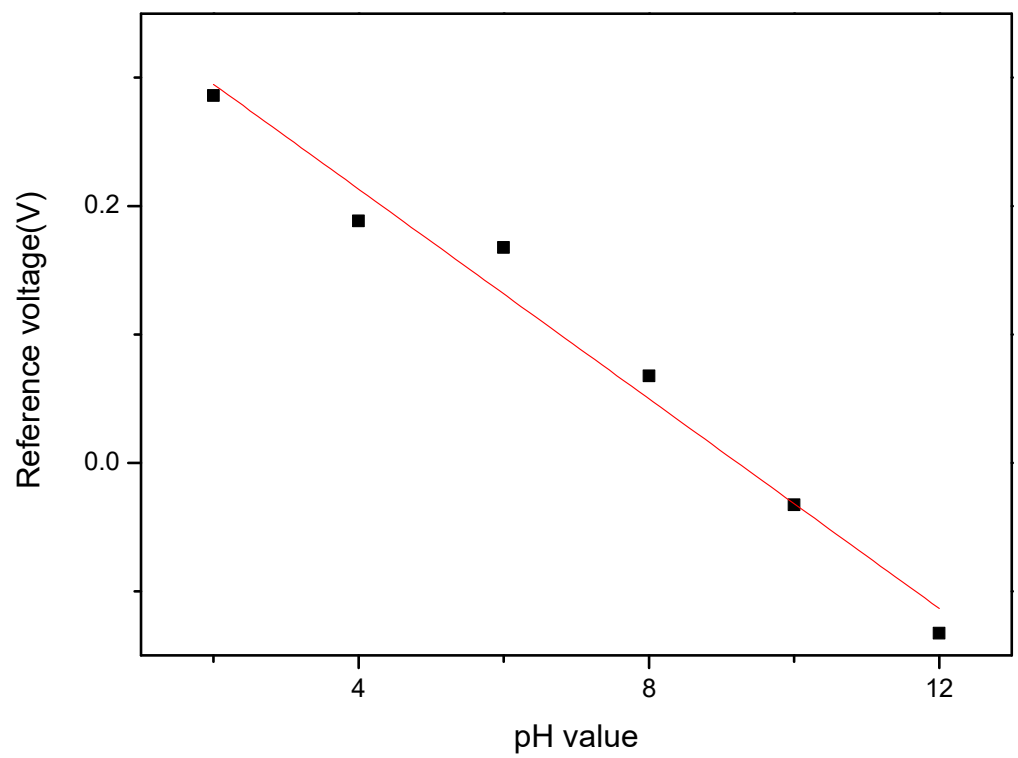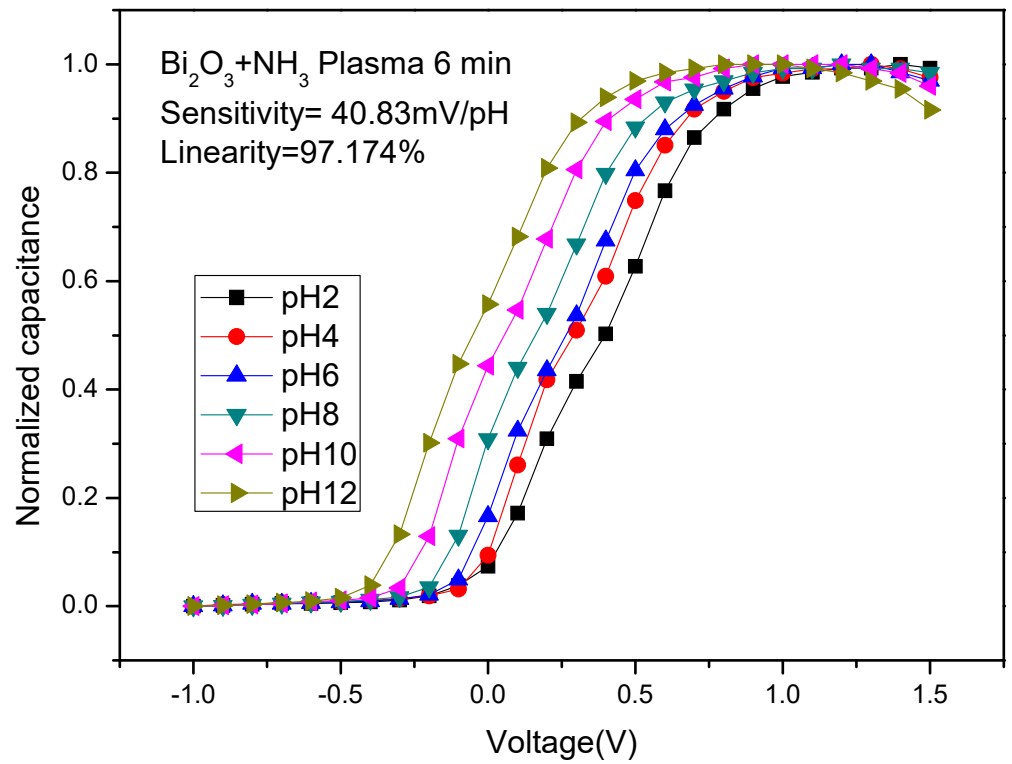

(**a**)

Figure 7. *Cont.*
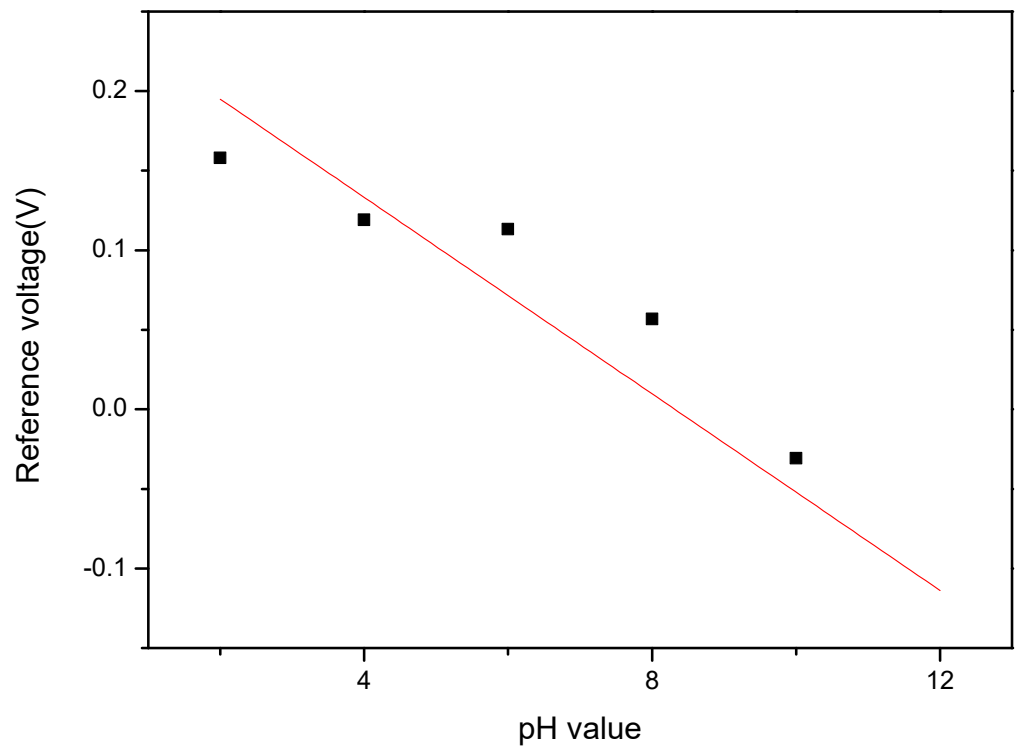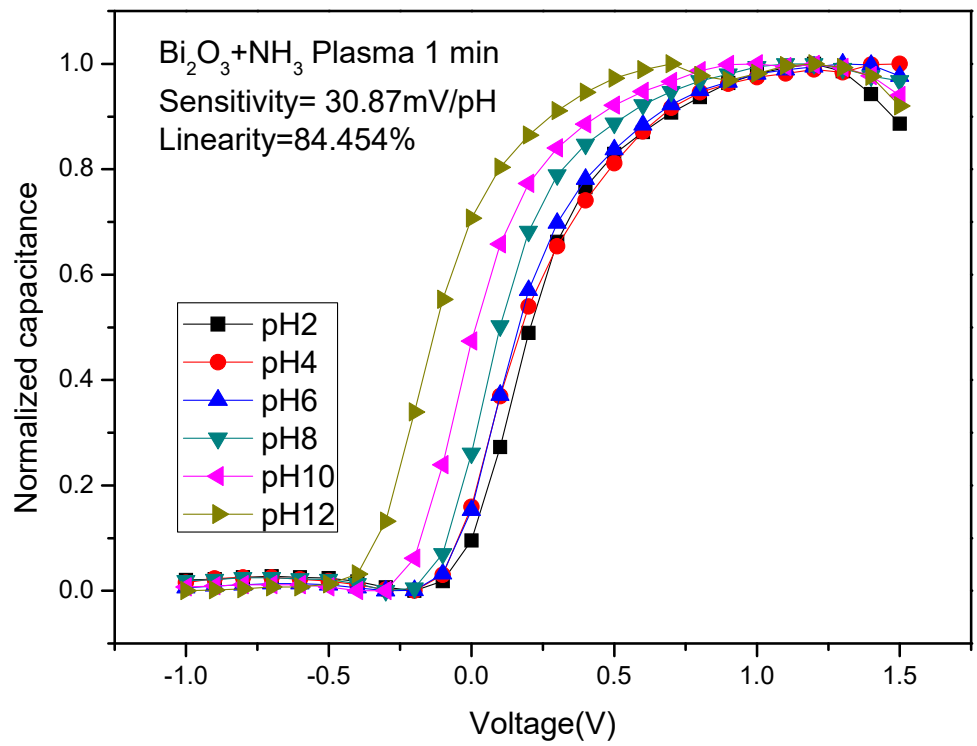
(**b**)

Figure 7. *Cont.*

(**c**)

Figure 7. *Cont.*

(**d**)

Figure 7. *Cont.*
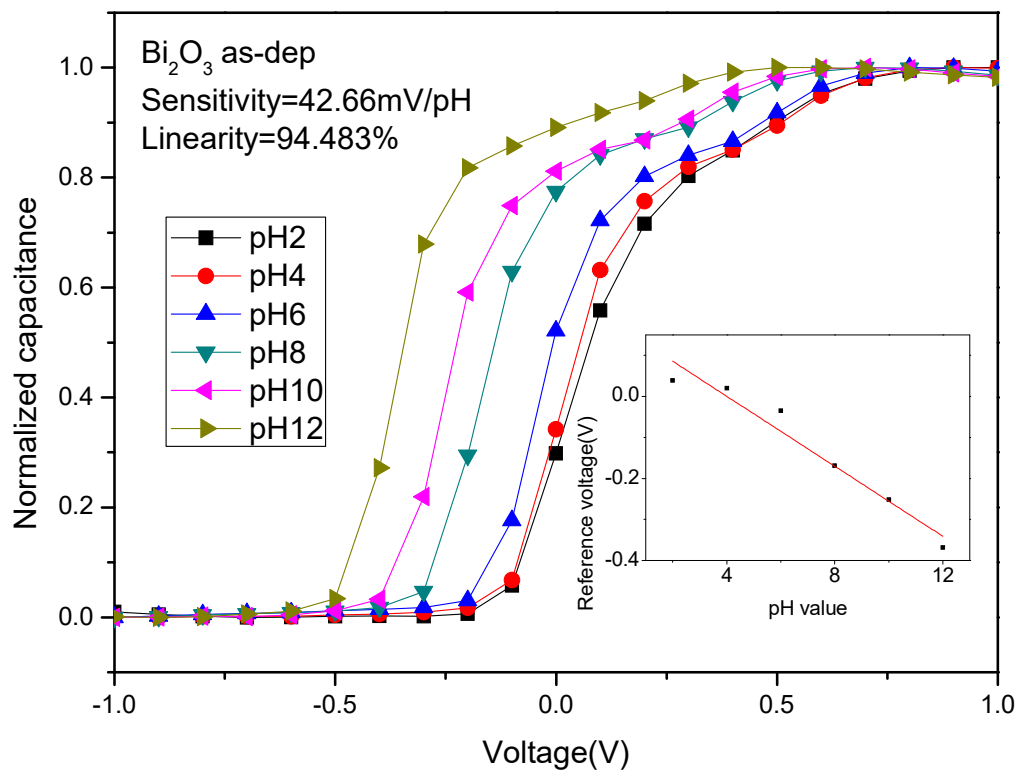
(**e**)
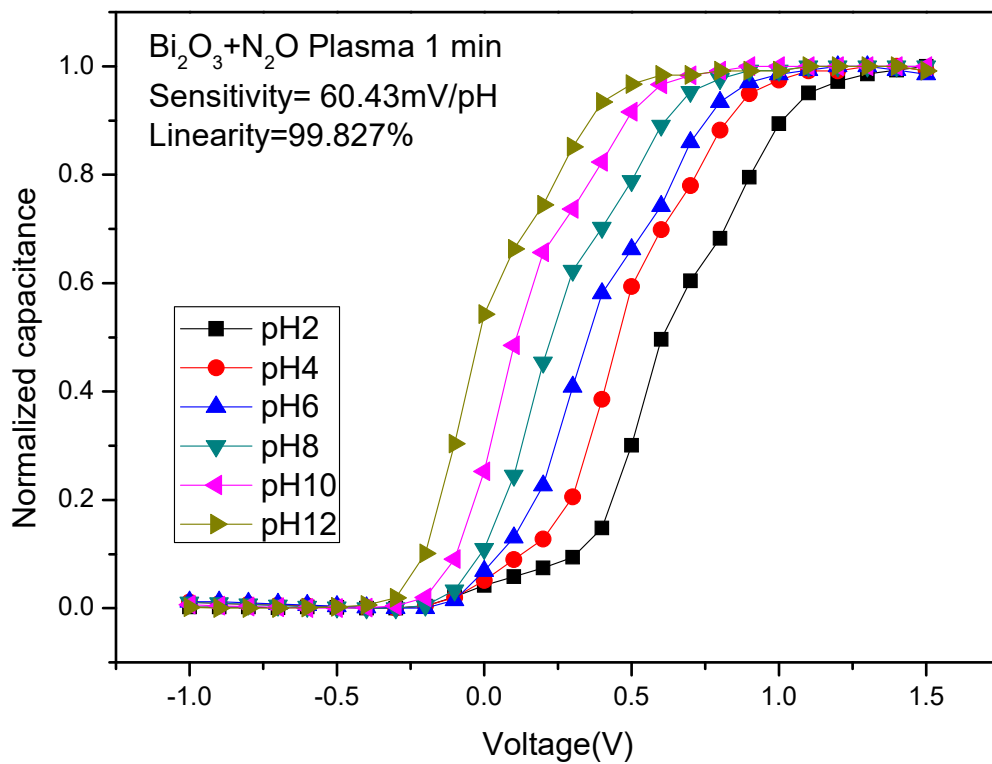
Figure 7. *Cont.*

(**f**)

Figure 7. *Cont.*

(**g**)

Bi$_2$O$_3$+N$_2$O Plasma 6 min
Sensitivity= 59.8mV/pH
Linearity=98.97%

Figure 7. *Cont.*

(**h**)
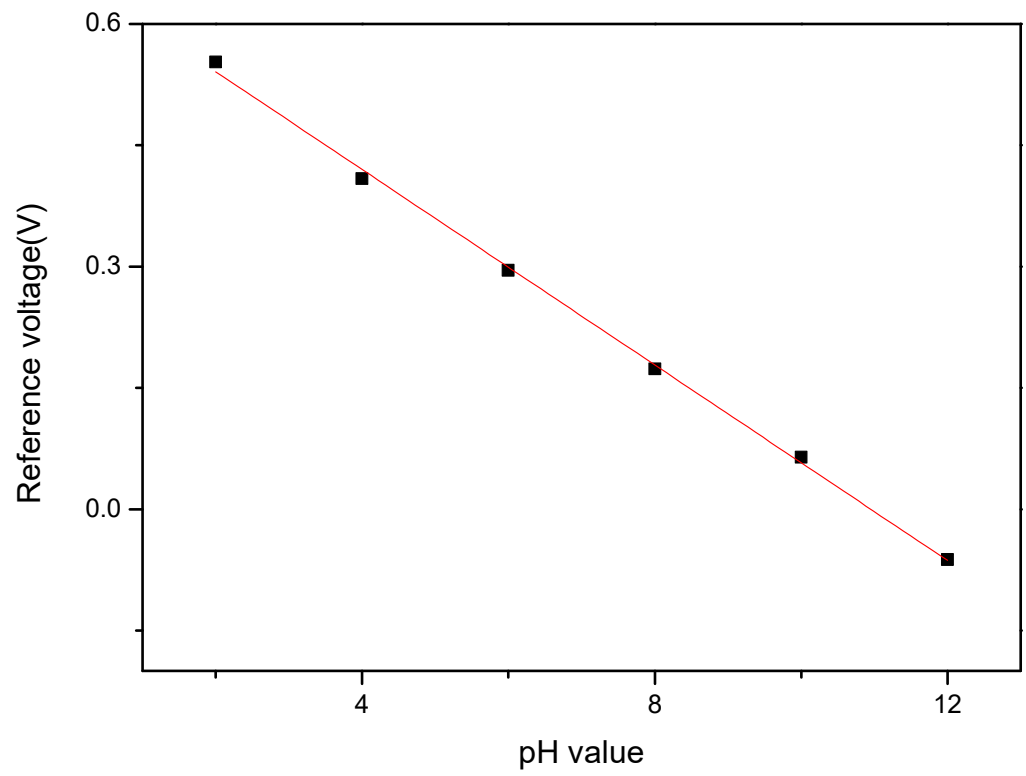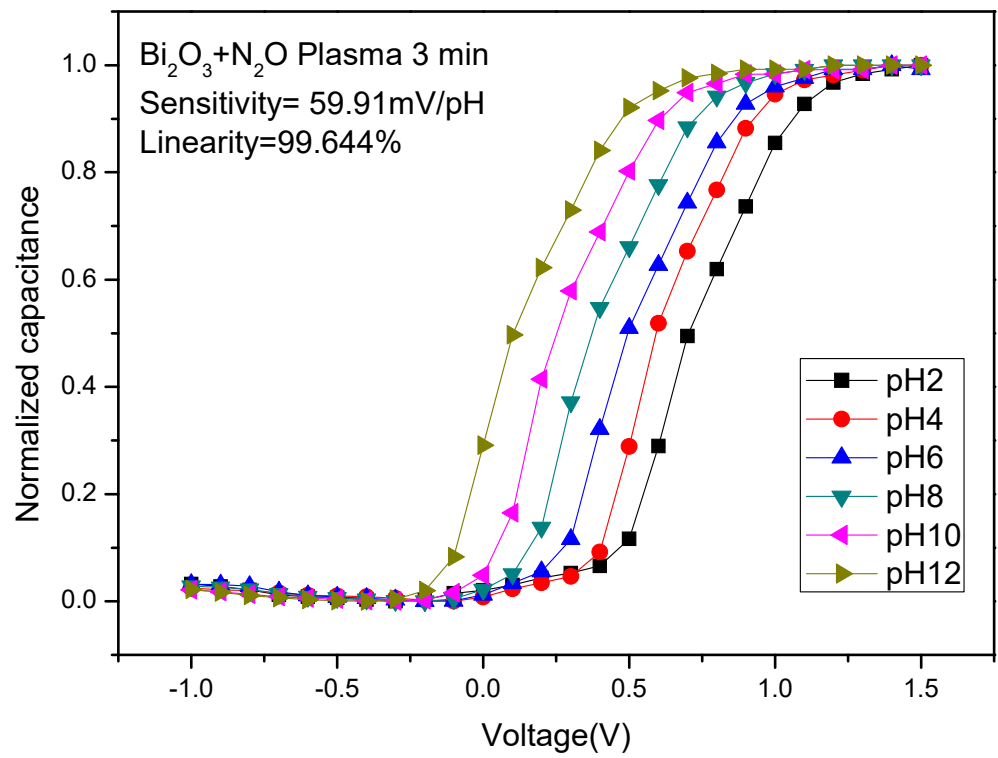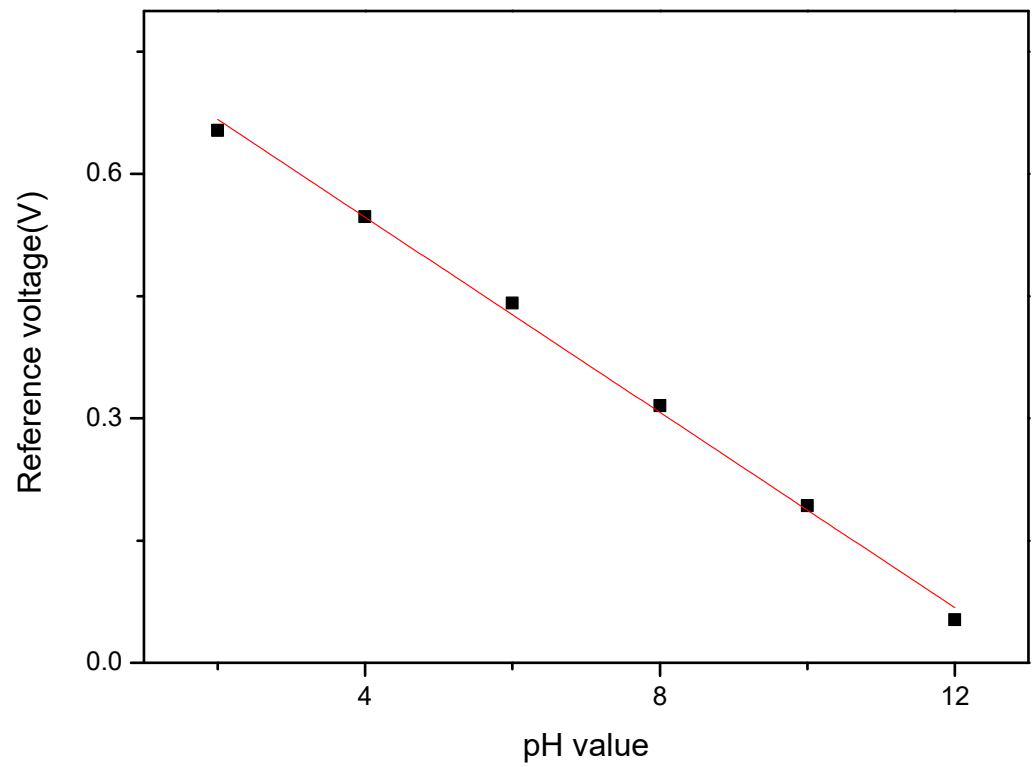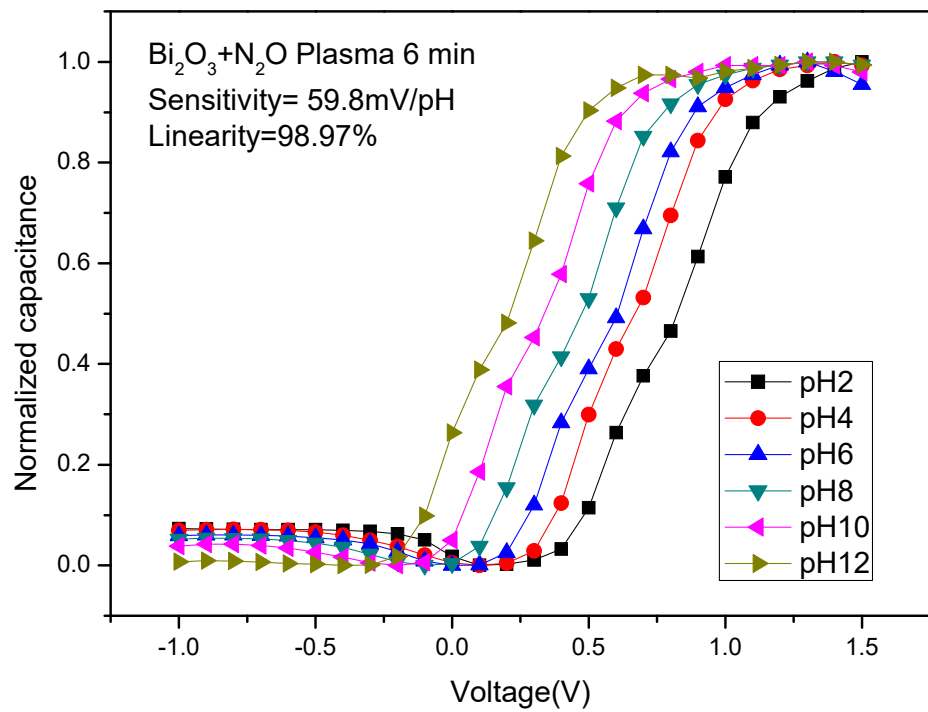
Figure 7. C–V curves of Bi_2O_3 sensing membrane with NH_3 plasma for (**a**) as-dep, (**b**) 1 min, (**c**) 3 min, (**d**) 6 min NH_3 plasma treatment. C–V curves of the Bi_2O_3 sensing membrane with N_2O plasma for (**e**) as-dep, (**f**) 1 min, (**g**) 3 min, (**h**) 6 min N_2O plasma treatment.
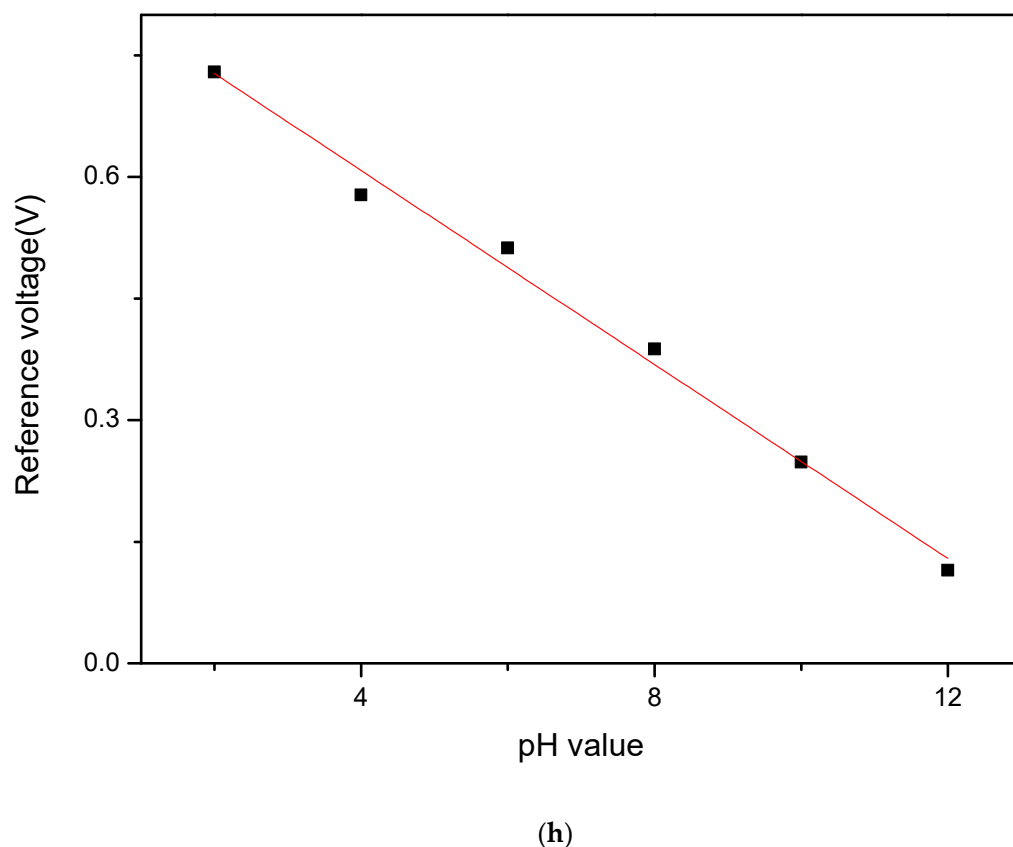
To investigate the reliability of the membranes, Figure 8a shows the hysteresis voltage of the Bi_2O_3 sensing film after NH_3 and N_2O plasma treatment. The Bi_2O_3 sensing film without plasma had a hysteresis voltage of 22.49 mV, and the hysteresis voltage after 1, 3, and 6 min of NH_3 plasma were 24.18, 3.31, and 16.13 mV, respectively. As for the Bi_2O_3 sensing film treated by NH_3 plasma at different times, the NH_3 plasma treatment for 3 min shows the lowest hysteresis voltage. Since the incorporation of N with NH_3 plasma treatment can passivate the defects, thereby inhibiting the diffusion of reactive ions and delaying the reference voltage response. Combined with the XPS analysis, it can be seen that the 3 min NH_3 plasma had the least oxygen vacancies, and the Bi-O bond was the strongest. After calculation, it can be known that the 3 min NH_3 plasma has the lowest Bi^{2+} content, so the sensor film shows low hysteresis voltage.
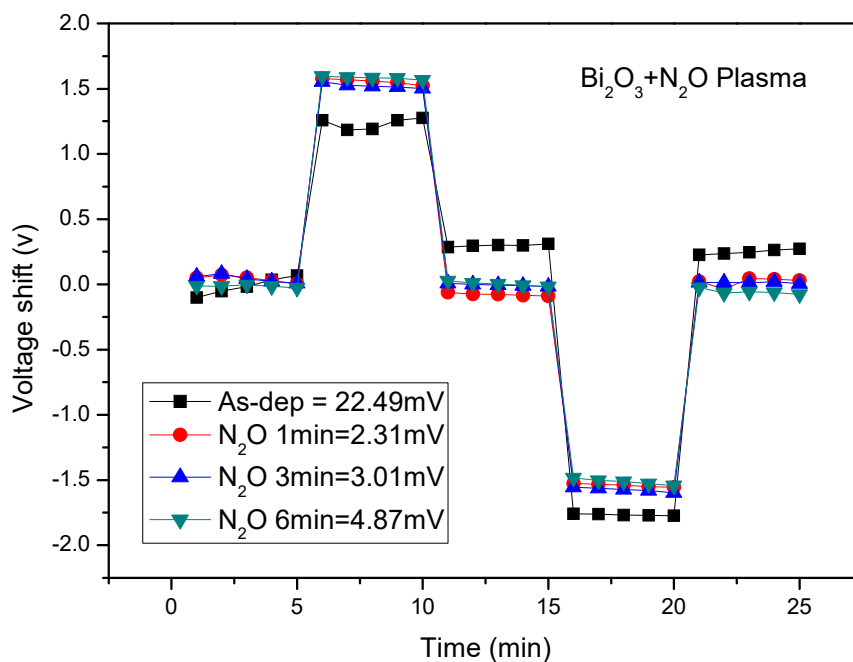
The hysteresis voltage of the Bi_2O_3 sensing film after N_2O plasma is shown in Figure 8b. The hysteresis voltage of the Bi_2O_3 sensing film without plasma was 22.49 mV, and the hysteresis voltage after 1, 3, and 6 min of N_2O plasma were 2.31, 3.01, and 4.87 mV, respectively. It was observed that after 1 min of N_2O plasma the membrane had a lower hysteresis voltage compared with all the other samples. As the plasma treatment time increased, the hysteresis voltage gradually increased because the crystals gradually became smaller, which caused the hysteresis voltage to rise.

Furthermore, Figure 8c,d shows the drift coefficient of the Bi_2O_3 sensing film after NH_3 and N_2O plasma, respectively. The drift coefficient is an important parameter describing the long-term stability of the sensor. In order to sense the long-term reliability of the film, we placed the Bi_2O_3 sensing film treated with plasma treatments in a pH7 solution for 12 h to obtain the drift rate of the sensing film. The drift rate of the Bi_2O_3 sensing film without plasma was 23.58 mV/hr, and the drift rate of the sensing film with NH_3 plasma after 1, 3, and 6 min were 20.7, 2.57, 15.09 mV/hr. It can be seen that the sensing film after 3 min

of NH_3 plasma had the lowest drift rate. This is because NH_3 plasma could effectively passivate the defects, which allow ions to adhere, thereby inhibiting the diffusion of reactive ions and varying the reference voltage response. Therefore, the drift rate was reduced. Figure 8d shows the drift coefficient of the Bi_2O_3 sensing film after N_2O plasma. The drift rate of Bi_2O_3 sensing film without plasma was 23.58 mV/hr, and the sensing film after N_2O plasma for 1, 3, and 6 min were 2.45, 3.44, and 7.57 mV/hr. The sensing film of N_2O plasma had the lowest drift rate in the sample with N_2O plasma for 1 min.
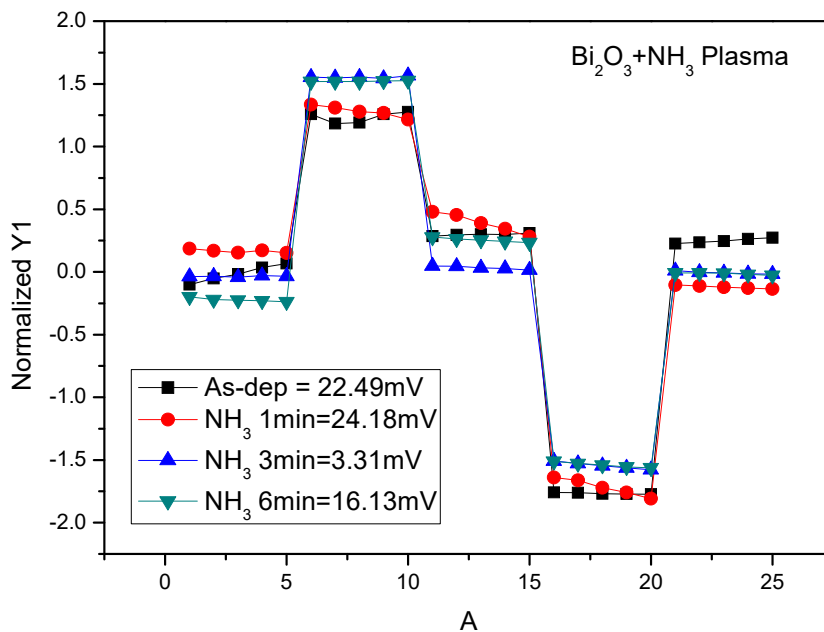
(**a**)

(**b**)

Figure 8. *Cont.*
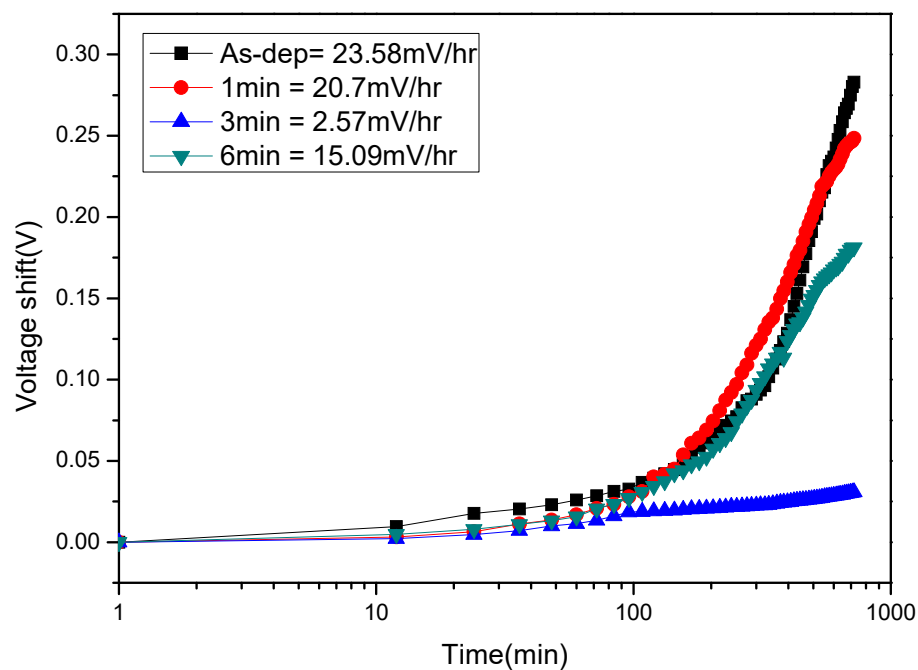
(**c**)
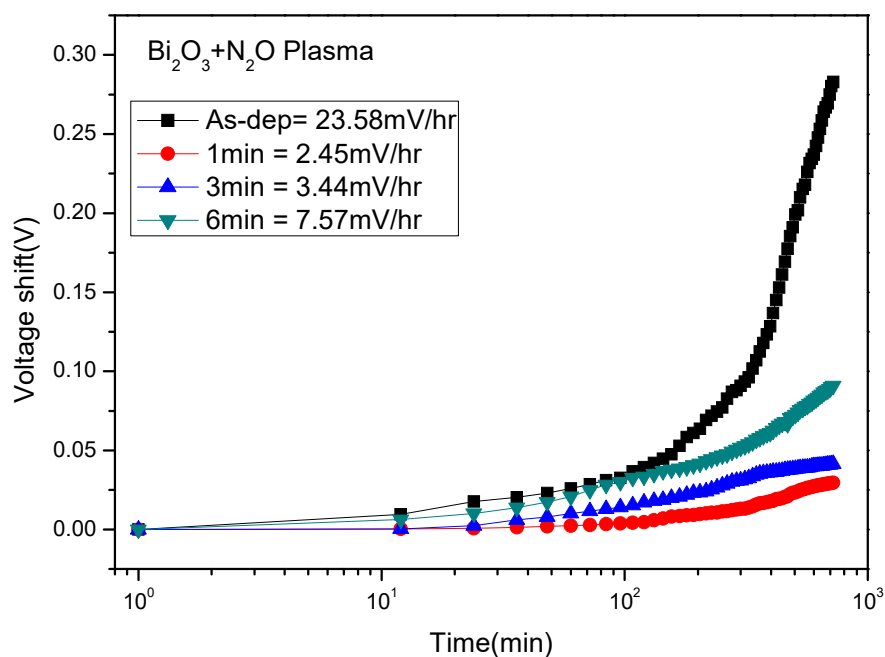
(**d**)

Figure 8. (**a**) Hysteresis voltage of the Bi_2O_3 sensing membrane after NH_3 plasma treatment during the pH loop of 7→4→7→10→7. (**b**) Hysteresis voltage of the Bi_2O_3 sensing membrane after N_2O plasma treatment during the pH loop of 7→4→7→10→7. (**c**) Drift voltage of the Bi_2O_3 sensing membrane after NH_3 plasma treatment, then dipped in pH 7 buffer solution for 12 h. (**d**) Drift voltage of the Bi_2O_3 sensing membrane after N_2O plasma treatment, then dipped in pH 7 buffer solution for 12 h.

4. Conclusions

Bi_2O_3 EIS sensing membranes in EIS structures were fabricated. To boost the sensing performance, NH_3 and N_2O plasma treatment were performed on the membranes. The results indicated that the sample treated with NH_3 plasma for 3 min and the sample with N_2O plasma treatment for 1 min had higher sensitivity than all the other conditions. Multiple material characterizations confirmed the enhancement of crystallization, and the removal of the defects may cause the improvements of the sensing behaviors owing to nitrogen passivation in the device. The plasma treatments could cause N atoms to incorporate into the bulks and the silicate could be transformed to well-crystallized films. Furthermore, plasma treatment could enhance grainization, which increased the density of the sensing surface sites, thereby boosting the sensing behaviors. Therefore, NH_3 or N_2O plasma treated-Bi_2O_3 membranes could reach the pH sensitivity around 60 mV/pH and show promise for future biomedical applications.

Author Contributions: Conceptualization, C.-H.K. and H.C.; methodology K.-L.C., C.-H.K. and H.C.; data curation, K.-L.C.; writing—original draft preparation, Y.-S.C., L.S.H., S.-M.C. and H.C.; writing—review and editing, M.-H.L., M.-L.L. and S.-M.C.; visualization, H.C.; supervision, M.-H.L., M.-L.L., C.-H.K. and H.C.; project administration, H.C.; funding acquisition, M.-L.L. and H.C. All authors have read and agreed to the published version of the manuscript.

Institutional Review Board Statement: Not applicable.

Data Availability Statement: Not applicable.

Conflicts of Interest: There are no conflict of interest to declare. The funders had no role in the design of the study; in the collection, analyses, or interpretation of data; in the writing of the manuscript, or in the decision to publish the result.

References

1. Bergveld, P. Development of an ion-sensitive solid-state device for neurophysiological measurements. *IEEE Trans. Biomed. Eng.* **1970**, *BME-17*, 70–71. [CrossRef] [PubMed]
2. Jeon, J.-H.; Cho, W.-J. High-performance extended-gate ion-sensitive field-effect transistors with multi-gate structure for transparent, flexible, and wearable biosensors. *Sci. Technol. Adv. Mater.* **2020**, *21*, 371–378. [CrossRef] [PubMed]
3. Karmakar, A.; Wang, J.; Prinzie, J.; De Smedt, V.; Leroux, P. A Review of Semiconductor Based Ionising Radiation Sensors Used in Harsh Radiation Environments and Their Applications. *Radiation* **2021**, *1*, 18. [CrossRef]
4. Al-Khalqi, E.M.; Hamid, M.A.A.; Shamsudin, R.; Al-Hardan, N.H.; Jalar, A.; Keng, L.K. Zinc Oxide Nanorod Electrolyte–Insulator–Semiconductor Sensor for Enhanced 2-Methoxyethanol Selectivity. *IEEE Sens. J.* **2020**, *21*, 6234–6240. [CrossRef]
5. Lee, K.H.; Chu, J.Y.; Kim, A.R.; Yoo, D.J. Effect of functionalized SiO2 toward proton conductivity of composite membranes for PEMFC application. *Int. J. Energy Res.* **2019**, *43*, 5333–5345. [CrossRef]
6. Samsudin, N.; Ferdaous, M.; Shahahmadi, S.; Mustafa, S.; Akhtaruzzaman, M.; Sopian, K.; Chelvanathan, P.; Amin, N. Deposition and characterization of RF-sputtered-Ta_2O_5 thin films for O_2 reduction reaction in polymer electrolyte membrane fuel cells (PEMFC). *Optik* **2018**, *170*, 295–303. [CrossRef]
7. Martins, A.S.; Lachgar, A.; Zanoni, M.V.B. Sandwich Nylon/stainless-steel/WO_3 membrane for the photoelectrocatalytic removal of Reactive Red 120 dye applied in a flow reactor. *Sep. Purif. Technol.* **2020**, *237*, 116338. [CrossRef]
8. Meng, D.; Zhao, Q.; Pan, X. Preparation of La_2O_3 by ion-exchange membrane electrolysis of $LaCl_3$ aqueous solution. *J. Rare Earths* **2019**, *37*, 1009–1014. [CrossRef]
9. Dmitrenko, M.; Penkova, A.; Atta, R.; Zolotarev, A.; Plisko, T.; Mazur, A.; Solovyev, N.; Ermakov, S. The development and study of novel membrane materials based on polyphenylene isophthalamide-Pluronic F127 composite. *Mater. Des.* **2019**, *165*, 107596. [CrossRef]
10. Jiang, L.; Yuan, X.; Zeng, G.; Liang, J.; Chen, X.; Yu, H.; Wang, H.; Wu, Z.; Zhang, J.; Xiong, T. In-situ synthesis of direct solid-state dual Z-scheme WO_3/g-C_3N_4/Bi_2O_3 photocatalyst for the degradation of refractory pollutant. *Appl. Catal. B Environ.* **2018**, *227*, 376–385. [CrossRef]

11. Nundy, S.; Eom, T.-y.; Song, K.-Y.; Park, J.-S.; Lee, H.-J. Hydrothermal synthesis of mesoporous ZnO microspheres as NOX gas sensor materials—Calcination effects on microstructure and sensing performance. *Ceram. Int.* **2020**, *46*, 19354–19364. [CrossRef]

12. Guo, X.; Zhao, X.; Liu, J.; He, W. Synthesis of Bismuth Doped Yttria Stabilized Zirconia Electrolyte and Study of Ionic Conductivity. 2021. Available online: https://assets.researchsquare.com/files/rs-479437/v1_covered.pdf?c=1631865568 (accessed on 29 December 2021).

13. Hu, X.; Zhu, X.; Wu, X.; Cai, Y.; Tu, X. Plasma-enhanced NH_3 synthesis over activated carbon-based catalysts: Effect of active metal phase. *Plasma Processes Polym.* **2020**, *17*, 2000072. [CrossRef]

14. Jõgi, I.; Erme, K.; Levoll, E.; Raud, J.; Stamate, E. Plasma and catalyst for the oxidation of NOx. *Plasma Sources Sci. Technol.* **2018**, *27*, 035001. [CrossRef]

15. Ghoneim, M.; Nguyen, A.; Dereje, N.; Huang, J.; Moore, G.; Murzynowski, P.; Dagdeviren, C. Recent progress in electrochemical pH-sensing materials and configurations for biomedical applications. *Chem. Rev.* **2019**, *119*, 5248–5297. [CrossRef] [PubMed]

16. Paredes-Madrid, L.; Fonseca, J.; Matute, A.; Gutiérrez Velásquez, E.I.; Palacio, C.A. Self-compensated driving circuit for reducing drift and hysteresis in Force Sensing Resistors. *Electronics* **2018**, *7*, 146. [CrossRef]

17. Lai, C.S.; Wu, W.C.; Chao, T.S.; Chen, J.H.; Wang, J.C.; Tay, L.-L.; Rowell, N. Suppression of interfacial reaction for HfO_2 on silicon by pre-CF_4 plasma treatment. *Appl. Phys. Lett.* **2006**, *89*, 072904. [CrossRef]

18. Wong, H.; Zhou, J.; Zhang, J.; Jin, H.; Kakushima, K.; Iwai, H. The interfaces of lanthanum oxide-based subnanometer EOT gate dielectrics. *Nanoscale Res. Lett.* **2014**, *9*, 472. [CrossRef]

19. Li, D.; Cui, X.; Du, M.; Zhou, Y.; Lan, F. Effect of Combined Hydrophilic Activation on Interface Characteristics of Si/Si Wafer Direct Bonding. *Processes* **2021**, *9*, 1599. [CrossRef]

20. Plawsky, J.; Gill, W.; Jain, A.; Rogojevic, S. Nanoporous dielectric films: Fundamental property relations and microelectronics applications. In *Interlayer Dielectrics for Semiconductor Technologies*; Elsevier: Amsterdam, The Netherlands, 2003; pp. 261–325.

21. Tin, N.P. Electrolyte-gated organic field effect transistor with functionalized lipid monolayer for novel sensors. *Appl. Phys. Express* **2020**, *13*, 011005.

22. Gohain, M.B.; Pawar, R.R.; Karki, S.; Hazarika, A.; Hazarika, S.; Ingole, P.G. Development of thin film nanocomposite membrane incorporated with mesoporous synthetic hectorite and MSH@ UiO-66-NH_2 nanoparticles for efficient targeted feeds separation, and antibacterial performance. *J. Membr. Sci.* **2020**, *609*, 118212. [CrossRef]

23. Lin, C.F.; Kao, C.H.; Lin, C.Y.; Chen, K.L.; Lin, Y.H. NH_3 Plasma-Treated Magnesium Doped Zinc Oxide in Biomedical Sensors with Electrolyte–Insulator–Semiconductor (EIS) Structure for Urea and Glucose Applications. *Nanomaterials* **2020**, *10*, 583. [CrossRef]

24. Oldham, K.B. A Gouy–Chapman–Stern model of the double layer at a (metal)/(ionic liquid) interface. *J. Electroanal. Chem.* **2008**, *613*, 131–138. [CrossRef]

25. Allagui, A.; Benaoum, H.; Olendski, O. On the Gouy–Chapman–Stern model of the electrical double-layer structure with a generalized Boltzmann factor. *Phys. A Stat. Mech. Appl.* **2021**, *582*, 126252. [CrossRef]

26. Klamminger, K. Installation and Optimisation of a Test Stand for Solid Oxide Fuel Cells and Solid Oxide Electrolyser Cells. Mater's Thesis, University of Leoben, Leoben, Austria, 2018.

27. Riley, A.; Nica, E. Internet of Things-based Smart Healthcare Systems and Wireless Biomedical Sensing Devices in Monitoring, Detection, and Prevention of COVID-19. *Am. J. Med. Res.* **2021**, *8*, 51–64.